



HAL
open science

Wave-filtering properties of elastically-asymmetric architected materials

Vladislav Yastrebov

► **To cite this version:**

Vladislav Yastrebov. Wave-filtering properties of elastically-asymmetric architected materials. 2019. hal-02394159

HAL Id: hal-02394159

<https://hal.science/hal-02394159>

Preprint submitted on 4 Dec 2019

HAL is a multi-disciplinary open access archive for the deposit and dissemination of scientific research documents, whether they are published or not. The documents may come from teaching and research institutions in France or abroad, or from public or private research centers.

L'archive ouverte pluridisciplinaire **HAL**, est destinée au dépôt et à la diffusion de documents scientifiques de niveau recherche, publiés ou non, émanant des établissements d'enseignement et de recherche français ou étrangers, des laboratoires publics ou privés.

Wave-filtering properties of elastically-asymmetric architected materials

Vladislav A. Yastrebov*

*MINES ParisTech, PSL Research University, Centre des Matériaux,
CNRS UMR 7633, BP 87, 91003, Evry, France*

(Dated: December 18, 2017)

We propose a class of metamaterials possessing an arbitrary strong elastic asymmetry, which emerges from contact interaction introduced in their architecture. The material can be made stiff in tension and soft in compression or vice versa. This asymmetry results in different wave celerities of tensile and compressive components of elastic waves. The faster component overtakes the slower one and results in their dissipative annihilation through high-frequency energy cascades. We discuss the mechanism of this damping, efficient signal-absorbing assemblies, and relevant material architectures.

PACS numbers: 46.55.+d,81.05.Zx,46.40.Cd,46.40.Ff

Mechanical behaviour of elastically asymmetric materials depends on the “directionality” of the strain tensor, i.e. on the signs of principal strains. For certain orientations $\boldsymbol{\sigma}(\boldsymbol{\varepsilon}) \neq -\boldsymbol{\sigma}(-\boldsymbol{\varepsilon})$, where $\boldsymbol{\sigma}$ is the Cauchy stress tensor and $\boldsymbol{\varepsilon}$ infinitesimal strain tensors. Therefore, the Young’s, shear and bulk moduli of such materials can depend on the loading direction. In addition to this asymmetry, elastic anisotropy can come in play. Such materials are rather common in nature and include granular materials, soils, materials with internal flaws (e.g. cracked rocks, concrete) and others [1]. In soft matter, living cells, due to elastic asymmetry of fibrin and collagen, are able to self-adjust in response to external loads [2–5]. However, for most solid materials the elastic asymmetry is rather small and is hard to control. The theoretical studies of quasi-static mechanical behaviour of such materials can be found in [1, 6–9]. The elastic wave propagation in asymmetric media was studied in [10–13]. Vibrational analyses of materials with internal impacts, which render them elastically asymmetric, were conducted in [14–16].

First, we propose a class of architected materials with elastic asymmetry, which emerges from internal contacts established between parts of the elemental cell (see Fig. 1). This asymmetry is controllable and invertible, non-destructive and arbitrary-strong, contrary to a marginal asymmetry occurring in natural solid materials. The idea behind this novel architecture is that the non-adhesive contact can bear only compressive loads and opens in case of tensile ones. This non-smooth and amplitude-independent non-linearity renders the internal contact a good candidate for widening or enhancing novel and meta properties of architected materials (see e.g. [17–19]). For example, if a zero-thickness cut is introduced in the material, as shown in Fig. 1(a), the resulting elastic modulus along OX direction depends on the sign of deformation: in case of tension, only thin ligaments bear the load and thus macroscopically the material behaves as a soft one; on the contrary, in compression, the contact in the cut is closed and can fully bear the load,

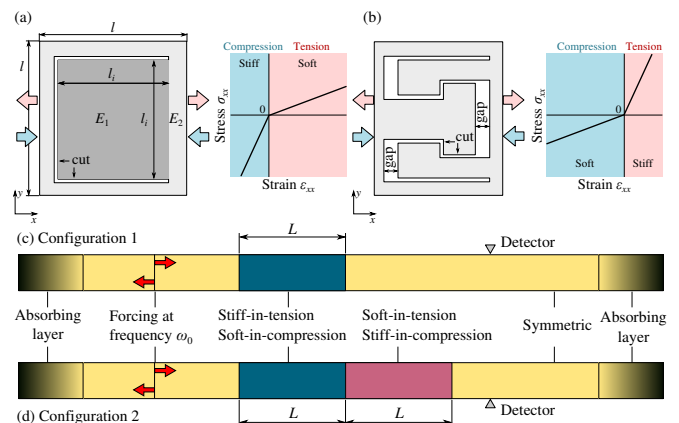


FIG. 1: (a,b) Examples of design of elemental architected cells with asymmetric elastic properties: the effective stiffness depends on the sign of horizontal strain component (compression/tension): architecture (a) is soft-in-tension and stiff-in-compression, architecture (b) is stiff-in-compression and soft-in-tension. The associated deformation curves are also shown. Configurations 1 and 2 depicted in (c) and (d), respectively are used to study 1D wave propagation in asymmetric media.

thus resulting in a stiffer elastic behaviour. The elastic asymmetry can be controlled by the dimensions of the cut and by materials used in the central and peripheral zones. For a simple design presented here, a rough estimation of the ratio of Young’s moduli in tension and compression can be given from simple geometrical consideration [20] by $E^+/E^- \approx (1 - l_i/l)E_2/E_1$, where l is the square-cell size, l_i is the side-length of Π -shape cut, and $E_{1,2}$ are Young’s moduli of the inner and outer materials: to amplify the asymmetry, materials can be chosen such that $E_1 > E_2$. Thus, the resulting asymmetry can greatly overpass the asymmetry of existing materials, which are stiffer in compression than in tension, such as rocks and concrete. The opposite asymmetry also occurs in Nature in fibrous materials [21–24] and living cells [4]: this asymmetry is based on local buckling of fibers under compression. In contrast to this mechanism, our architecture uses contact interaction to achieve comparable property. A novel stiff-in-tension and soft-in-compression architec-

ture is presented in Fig. 1(b): the contact is activated in tension and renders the material stiffer than in compression; in the latter case only thin ligaments bear the load as far as the gap remains open [see Fig. 1(b)]. The asymmetry of this material can be also enhanced by combination of stiff and soft materials in the architecture.

Such materials demonstrate unusual properties in dynamics both in vibration and wave propagation [13, 15, 25]. The latter presents the main topic of this paper. Namely, we study propagation of elastic waves through a one-dimensional assembly of symmetric and asymmetric materials, the focus is put on the damping properties. We show that the elastic asymmetry modifies the energy dissipation mechanisms, ensuring rapid damping for even low-frequency signals.

A one-dimensional wave equation for longitudinal waves propagating through a bi-modulus elastic material [10] with viscous dissipation of Kelvin-Voigt type (an elastic spring connected in parallel with a damper) [26] is of the form:

$$\rho u_{,tt} = E(u_{,x} + \alpha|u_{,x}|)_{,x} + \mu u_{,xxt}, \quad -1 < \alpha < 1, \quad (1)$$

where u is the horizontal displacement, lower indices after comma denote partial derivation $\bullet_{,x}$ and $\bullet_{,t}$ with respect to coordinate and time, respectively; ρ is the mass density (kg/m^3), E is the elastic modulus (Pa), and μ is the viscosity (Pa.s). The adimensional factor α determines the material asymmetry: the elastic modulus is equal to $E^+ = E(1 + \alpha)$ and $E^- = E(1 - \alpha)$ in tension ($u_{,x} > 0$) and compression ($u_{,x} < 0$), respectively. Thus, the tensile and compressive components of elastic waves propagate at celerities $c^\pm = \sqrt{E^\pm/\rho}$, respectively. Note that for a signal which has either purely compressive or tensile deformation, the wave propagation is governed by a linear Kelvin-Voigt model, however the superposition principle for deformation of different signs does not hold. The behaviour is independent of the signal amplitude since the non-linearity is localized in a single point on deformation curve (change of sign), which is centred at zero deformation. For one-dimensional systems, *elastic asymmetry* reduces to *bi-modulus* material model, thus hereinafter these two terms will be used interchangeably.

We consider propagation of elastic waves in structures shown in Fig 1(c,d) which include one or two sections with bi-modulus materials. Oscillations are induced at an excitation point in an elastically symmetric section of a bar by applying a harmonic force $f = f_0 \sin(\omega_0 t)$. Forcing frequency ω_0 is chosen in the interval in which viscous effects are almost negligible, i.e. $\mu\omega_0/\rho c^{\pm 2} \ll 1$. The induced elastic weakly-dispersive waves propagate to the left and to the right: on the left they are absorbed by an absorbing layer. On the right they pass through a single section of length L of bi-modulus material [*Configuration 1*, see Fig. 1(c)], which without loss of generality can be considered to be stiff-in-tension and

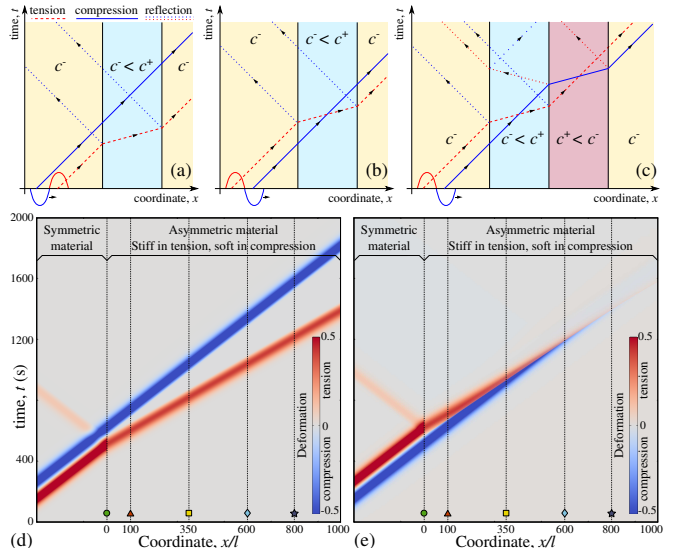


FIG. 2: Spatio-temporal wave tracing is presented in (a) for a tensile component (dashed line) followed by a compressive one (solid line), (b) inverse incident signal, (c) inverse incident signal passing through a configuration with sections of opposite asymmetries; (a,b) and (c) correspond to Configuration 1 and 2, respectively [see Fig. 1(c,d)]. Simulation results for $\alpha = 0.3$, $\mu/\rho = 0.01 \text{ m}^2/\text{s}^2$, $E/\rho = 1 \text{ m/s}$: (d) and (e) represent spatio-temporal deformation map ($u_{,x}$) and correspond to the diagram (a) and (b), respectively; $x/l = 0$ separates symmetric and asymmetric sections.

soft-in-compression, i.e. $\alpha_1 > 0$ and $E_1^+ > E_1^-$. In addition, we consider *Configuration 2* [see Fig. 1(d)], which has an extra section of a bi-modulus material with the opposite asymmetry, i.e. it is soft-in-tension and stiff-in-compression ($\alpha_2 = -\alpha_1 < 0$, $E_2^+ < E_2^-$). The bi-modulus section(s), are followed by a symmetric elastic bar with another absorbing layer on its extremity. The equations of motion are solved numerically using finite differences and Störmer-Verlet integrator, see Supplementary material [27]. The spatial discretization unit l reflects the size of the architected elemental cell, thus the boundaries between symmetric and asymmetric sections pass between two springs separated by the concentrated mass. If $\lambda_0 \gg l$ (where λ_0 is a signal wavelength), such a homogenized model represents an effective medium for asymmetric architected materials with internal contacts. The model is less reliable for short wavelengths $\lambda/l \sim 1$, but can be viewed as a first order approximation.

Consider Configuration 1 [Fig. 2(a,d)] with a single wave $u_{,t}(x,t) = -v_0 \sin(\omega_0(x/c_0 - t))H(t - x/c_0)H(x/c_0 - t + 2\pi/\omega_0)$ propagating from left to right if $\omega_0 > 0$ at celerity c_0 , $H(\bullet)$ here denotes the Heaviside function, which is used to isolate a single wave [28]. In this wave the tensile component is followed by a compressive one. We assume, that the elastic modulus of the symmetric section is equal to the compressive modulus of the bi-modulus material $E_0 = E^-$ and $c_0 = c^-$.

When this single wave enters the bi-modulus section, the tensile component accelerates abruptly and propagates at celerity $c^+ > c^-$, whereas the compressive component continues to propagate at the same celerity c^- and passes smoothly from symmetric to bi-modulus section, and further to symmetric section. In contrast, the tensile component is partly reflected back towards the emitter because of the elastic contrast: it occurs in entering and escaping the bi-modulus section. Within the bi-modulus section, because of the difference in wave celerity of the compressive and tensile components, at re-entering into elastically symmetric zone, these two components are separated by $\Delta t = L/(c^+ - c^-)$ in time and by $\Delta x = L/(1 - c^-/c^+)$ in space. These properties can be used to construct a wave filter, which (1) due to reflection can partly attenuate the passage of either tensile or compressive wave components, and (2) due to contrast in celerities can separate the tensile and compressive components in space/time.

If the order of wave components is reversed [Fig. 2(b,e)], i.e. $\omega_0 < 0$, then the compressive component precedes the tensile one, and the system dynamics is more complex. The slow leading component is overtaken by the faster tensile one and they start to interfere. Note that contrary to the purely symmetric case considered in [13], the ratio of amplitudes of the tensile and compressive components propagating in the bi-modulus section is given by $A^+/A^- = 2/(1+c^+/c^-)$ (due to reflection), and their wavelengths relate as $\lambda^-/\lambda^+ = c^-/c^+$. The overlap process leads to emergence of high frequency oscillations and accompanying viscous dissipation, which results in partial or almost complete annihilation of tensile and compressive wave components [see Fig. 2(e)]. However, these oscillations do not necessarily imply high-frequency alteration between tension and compression. In the first stage they simply superpose with the compressive wave [29]. Since in Kelvin-Voigt model the amplitude of a wave with a real wavenumber k decays in time t as $\exp(-\mu k^2 t/2\rho)$; in the limit of high wavenumber $k > 2c^\pm/\mu$, the waves are overdamped and the harmonic part fully disappears. At later stages, the oscillations produced by the overlap of tensile and compressive components lead to frequent alteration of the deformation sign. As known [14, 15], oscillators with piecewise smooth characteristics possess sub-harmonic resonances at higher frequencies, which ensure relatively high amplitude and enhanced dissipation.

It is straightforward to find a propagation distance L_o needed for the tensile and compressive parts of initially harmonic signal to superpose completely. We introduce the following notations: $E_{\max} = \max\{E^+, E^-\}$, $E_{\min} = \min\{E^+, E^-\}$ and $c_{\max} = \max\{c^+, c^-\}$, $c_{\min} = \min\{c^+, c^-\}$, the material contrast is then denoted by $\gamma = E_{\max}/E_{\min} = (1+|\alpha|)/(1-|\alpha|) > 1$ and $c_{\max}/c_{\min} = \sqrt{\gamma}$. The overlap distance depends on wave celerities in the bi-modulus section and on the initial separation

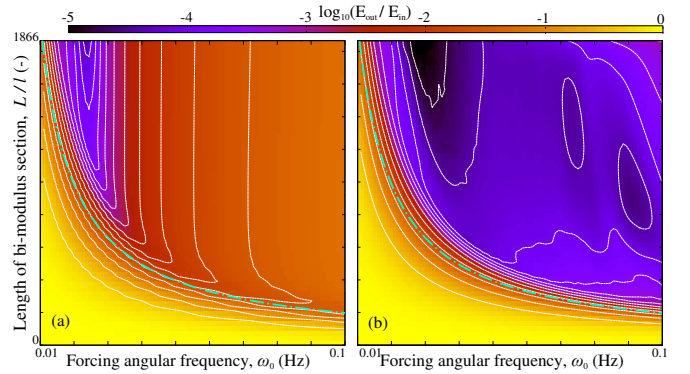


FIG. 3: The decimal logarithm of the ratio of transmitted to incident energy is plotted for different forcing frequencies ω_0 and different lengths of bi-modulus section L : (a) Configuration 1 [see Figs. 1(c),2(d)], (b) Configuration 2 [see Figs. 1(d),2(e)]. Dashed curves mark transmission iso-levels, dash-dotted curves represent Eq. (2).

in time of tensile and compressive components, which is equal to a half of the period $\Delta T = \pi/\omega_0$ in the symmetric section (where the oscillations are forced). Equating the length needed for faster and slower waves to travel to the same spatio-temporal point and requiring the full-period overlap, we obtain the overlap distance

$$L_o = \frac{2\pi c_{\max}}{\omega_0(\sqrt{\gamma} - 1)} \quad (2)$$

If the symmetric section is stiff $c_0 = c_{\max}$, then the overlap distance is given by $L_o = \lambda_0/(\sqrt{\gamma} - 1)$; if $c_0 = c_{\min}$ then $L_o = \lambda_0 + \lambda_0/(\sqrt{\gamma} - 1)$.

The high-frequency cascades emerging in annihilation of tensile and compressive waves present a powerful dissipative and filtering mechanism. To test its properties we analyse the energy passing through the bi-modulus section(s) as a function of its length and forcing frequency ω_0 . The injected energy is computed as the work of the imposed force $E_{\text{in}} = \int_0^T f(t)u_t dt/2$ [30], where T is the forcing time. The transmitted energy is computed right after the bi-modulus section(s) [see detector in Fig. 1(c,d)] as accumulated energy E_{out} passing through a single elemental volume $E_{\text{out}} = \int_{T_1}^{T_2} [E_{k,t} + E_{p,t}] dt$, where $E_{k,t}, E_{p,t}$ are the power of kinetic and potential energies, respectively. The time interval $[T_1, T_2]$ is chosen such to grasp all waves and most of reflections excited by the incident signal. Because of the absorbing layer on the far-right end of the structure, the energy integrated over time is equal to the energy passed from left to right within the given time interval.

The ratio of transmitted to incident signal energy $\log_{10}(E_{\text{out}}/E_{\text{in}})$ is plotted in Fig. 3(a,b) as a function of the forcing frequency ω_0 and the length of the bi-modulus section L , for Configurations 1 and 2, respectively. The following parameters were used $E/\rho = 1$ (m^2/s^2), elemental cell length is $l = 1$ (m) and area $A = 1$ (m^2), $\alpha = 0.3$, $\mu/\rho = 0.01$ (m^2/s^2). For Configuration 1, the

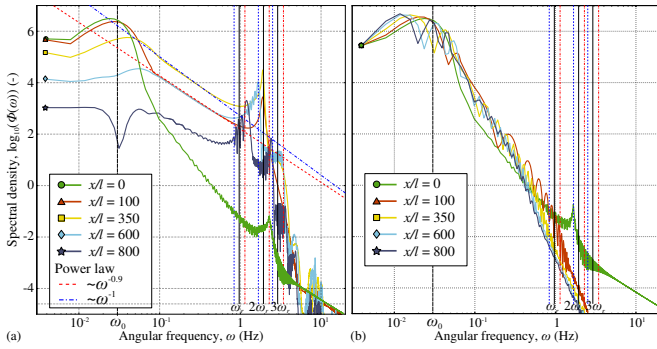


FIG. 4: Spectral density $\Phi(\omega)$ at locations marked in Fig. 2(d,e). (a) Configuration 1, scenario of Fig. 2(b,e). Initial peak at the incident frequency ω_0 is visible, as well as an emerging high frequency peak at sub-resonance frequency $2\omega_r$. High-energy cascade with an exponent in the interval $[0.9, 1]$ is highlighted. (b) Spectral density remains almost constant for Configuration 1, scenario of Fig. 2(a,d) for separating tensile and compressive wave components.

transmitted energy reduces significantly if the length of bi-modulus section is greater than the overlap length L_o given in Eq. (2). For Configuration 2, the same qualitative effect is observed, however, it is greatly amplified [31] by the bi-modulus section of the same length L but with the opposite asymmetry, which is introduced right after the first bi-modulus section. After the first (partial) annihilation of tensile and compressive waves, the remnants of the tensile component precedes the compressive ones [see also Fig. 2(d)]. The second section with the inverse asymmetry serves to collide them again and dissipate their energy. Multiple combinations of antisymmetric sections can be used to ensure even more efficient damping as long as within every section tensile and compressive components overtake each other, i.e. the length of the section is greater than the overlap length $L \geq L_o$ (see Eq. (2)). From Eq. (2) and the simulation data it follows that the absorption is very efficient for high and low frequency as long as $\omega_0 > 2\pi c_{\max}/L(\sqrt{\gamma} - 1)$. A similar damping shall occur for a random wave packet, which contains a roughly equal proportion of tensile and compressive components which “annihilate” via the same mechanism.

The presence of high-frequency energy cascades can be shown through spectral analysis. In Fig. 4 the evolution of the spectral density of deformation u_x is shown for the cases depicted in Fig. 2(a,d and b,e). It is computed at several locations x along the bi-modulus section [marked in Fig. 2(d,e)] for the whole time history as $\Phi(\omega, x) = \hat{u}_x \hat{u}_x^*$, where $\hat{u}_x(\omega, x) = \int_0^\infty e^{-i\omega t} u_x(x, t) dt$ is the temporal Fourier transform, $\hat{\bullet}^*$ denotes the conjugate value, and ω is the angular frequency. We assume that at $t < 0$ the studied system is at rest. The system is forced mainly at frequency $\omega_0 = 0.03$ Hz, resulting in a smooth peak in Φ for the signal entering the bi-modulus section at $x = 0$. Note that the resonance frequencies of the bi-modulus element is given by

$\omega_r = 2j\sqrt{1 - \alpha^2}/(\sqrt{1 - \alpha} + \sqrt{1 + \alpha})\sqrt{E_0/\rho l^2}$ (see, [16]), where the main resonance occurs for $j = 1$ and high-frequency sub-harmonic resonances occur at $j > 1$ and $j \in \mathbb{N}$. In the signal spectrum [Fig. 4(a)] for the case of wave overlap [Fig. 2(b,e)], a second peak emerges at $j = 2$ sub-harmonic frequency of elemental cells. This peak, which grows with the propagation distance, presents a sink for the energy transmitted from low frequencies. The energy spectrum thus contains two peaks connected via a power law decay section with the exponent between -1.0 and -0.9 as shown in Fig. 4(c). Note that the energy decay of the main frequency ω_0 , as well as the rise and subsequent decay of sub-frequencies $n\omega_0$, for $n \in \mathbb{N}, n > 1$ is consistent with the findings presented in [13], where the main features of this dissipation were grasped. In contrast, when tensile and compressive components separate [Fig. 2(a,d)], the spectrum depicted in Fig. 4(b) does not present any particularities and the energy content remains rather stable.

In conclusion, we proposed new architected materials in which the elastic asymmetry can be finely adjusted by combining internal contacts and components of different stiffness. Further, we studied the propagation of one-dimensional elastic waves in the resulting elastically asymmetric media. We found that the overlap of tensile and compressive wave components propagating at different celerities results in emergence of high-frequency energy cascades. It can be seen as tensile-compressive wave annihilation, which presents a novel and powerful signal damping mechanism. Moreover, it is enhanced drastically if a section with one asymmetry is followed by another one with the opposite asymmetry. The efficient wave damping is ensured if the bi-modulus section is chosen longer than the wave-overlap length (2). The ratio of the overlap length to the incident wavelength scales as $L_o/\lambda_0 \sim 1/(\sqrt{\gamma} - 1)$. The key advantage of the proposed architected materials consists in fact that the elastic asymmetry γ can be adjusted to be high, which would enable to keep the damping device relatively small compared to the characteristic incident wavelength.

The demonstrated efficient damping mechanism can be used in shock absorbing systems, and, potentially, in seismic protection from surface waves. The one-dimensional model presented here can be extended to two and three dimensional cases, where the compressive/tensile elastic asymmetry should be enhanced with shear asymmetry and complemented by elastic anisotropy.

Acknowledgement. The author is grateful to Lev Truskinovsky for valuable discussions, to Samuel Forest for his encouragement, and to Arsen Subashiev for helpful remarks to the text.

* vladislav.yastrebov@mines-paristech.fr

- [1] R. M. Jones, *AIAA Journal* **15**, 16 (1977).
- [2] N. Wang, K. Naruse, D. Stamenović, J. J. Fredberg, S. M. Mijailovich, I. M. Tolić-Nørrelykke, T. Polte, R. Mannix, and D. E. Ingber, *Proc. Natl. Acad. Sci. U.S.A.* **98**, 7765 (2001).
- [3] P. A. Janmey, M. E. McCormick, S. Rammensee, J. L. Leight, P. C. Georges, and F. C. MacKintosh, *Nat. Mater.* **6**, 48 (2007).
- [4] J. Notbohm, A. Lesman, P. Rosakis, D. A. Tirrell, and G. Ravichandran, *Journal of The Royal Society Interface* **12**, 20150320 (2015).
- [5] P. Ronceray, C. P. Broedersz, and M. Lenz, *Proc. Natl. Acad. Sci. U.S.A.* **113**, 2827 (2016).
- [6] S. A. Ambartsumyan and A. A. Khachatryan, *Mech. Solids* **1**, 29 (1966).
- [7] A. Curnier, Q.-C. He, and P. Zysset, *J. Elast.* **37**, 1 (1994).
- [8] J.-y. Sun, H.-q. Zhu, S.-h. Qin, D.-l. Yang, and X.-t. He, *J. Mech. Sci. Technol.* **24**, 1845 (2010).
- [9] S. Nemat-Nasser and M. Hori, *Micromechanics: overall properties of heterogeneous materials*, Vol. 37 (Elsevier, 2013).
- [10] V. P. Maslov and P. P. Mosolov, *J. Appl. Math. Mech.* **49**, 322 (1985).
- [11] S. Lepri and G. Casati, *Phys. Rev. Lett.* **106**, 164101 (2011).
- [12] S. N. Gavrilov and G. C. Herman, *J. Sound Vib.* **331**, 4464 (2012).
- [13] A. Radostin, V. Nazarov, and S. Kiyashko, *Wave Motion* **50**, 191 (2013).
- [14] J. M. T. Thompson and R. Ghaffari, *Phys. Lett. A* **91**, 5 (1982).
- [15] S. Natsiavas, *J. Sound Vib.* **165**, 439 (1993).
- [16] R. V. Goldstein, S. V. Kuznetsov, and M. A. Khudiyakov, *Mech. Solids* **50**, 294 (2015).
- [17] D. M. Kochmann and W. J. Drugan, *J. Mech. Phys. Solids* **57**, 1122 (2009).
- [18] P. Wang, F. Casadei, S. Shan, J. C. Weaver, and K. Bertoldi, *Phys. Rev. Lett.* **113**, 014301 (2014).
- [19] B. Florijn, C. Coulais, and M. van Hecke, *Phys. Rev. Lett.* **113**, 175503 (2014).
- [20] In this estimation we assumed that $l_i \approx l$.
- [21] O. Lourie, D. M. Cox, and H. D. Wagner, *Phys. Rev. Lett.* **81**, 1638 (1998).
- [22] A. Sears and R. C. Batra, *Phys. Rev. B* **69**, 235406 (2004).
- [23] L. R. Meza, S. Das, and J. R. Greer, *Science* **345**, 1322 (2014).
- [24] J. Dirrenberger, S. Forest, and D. Jeulin, *Int. J. Solids Struct.* **51**, 359 (2014).
- [25] V. Tournat and V. E. Gusev, *Phys. Rev. E* **80**, 011306 (2009).
- [26] A. C. Eringen, *Mechanics of continua* (Huntington, NY, Robert E. Krieger Publishing Co., 1980).
- [27] V. A. Yastrebov, "Supplementary material," (2017).
- [28] We used a Gaussian smoothing of signal tails to avoid high frequency oscillations.
- [29] Note that these oscillations do not emerge if tensile and compressive waves going in opposite directions pass through each other.
- [30] The factor 1/2 appears here since only a half of the energy goes towards the bi-modulus section, the other part goes to the left towards the absorbing layer.
- [31] In average the double layer enables to absorb two orders of magnitude more energy than a single layer.